Analyst

PAPER

View Article Online
View Journal | View Issue

Cite this: *Analyst*, 2023, **148**, 839

Smartphone-read phage lateral flow assay for point-of-care detection of infection†

Maede Chabi,[a] Binh Vu,[b] Kristen Brosamer,[a] Maxwell Smith,‡[b] Dimple Chavan,§[c] Jacinta C. Conrad,*[b] Richard C. Willson*[a,b,c,d] and Katerina Kourentzi*[b]

The COVID-19 pandemic has highlighted the urgent need for sensitive, affordable, and widely accessible testing at the point of care. Here we demonstrate a new, universal LFA platform technology using M13 phage conjugated with antibodies and HRP enzymes that offers high analytical sensitivity and excellent performance in a complex clinical matrix. We also report its complete integration into a sensitive chemiluminescence-based smartphone-readable lateral flow assay for the detection of SARS-CoV-2 nucleoprotein. We screened 84 anti-nucleoprotein monoclonal antibody pairs in phage LFA and identified an antibody pair that gave an LoD of 25 pg mL^{-1} nucleoprotein in nasal swab extract using a FluorChem gel documentation system and 100 pg mL^{-1} when the test was imaged and analyzed by an in-house-developed smartphone reader. The smartphone-read LFA signals for positive clinical samples tested (N = 15, with known Ct) were statistically different ($p < 0.001$) from signals for negative clinical samples (N = 11). The phage LFA technology combined with smartphone chemiluminescence imaging can enable the timely development of ultrasensitive, affordable point-of-care testing platforms for SARS-CoV-2 and beyond.

Received 10th September 2022,
Accepted 4th January 2023

DOI: 10.1039/d2an01499h

rsc.li/analyst

1. Introduction

The global health crisis of COVID-19 revealed an urgent need for sensitive, rapid and easily deployable diagnostic tests for the detection of active infection.[1,2] Rapid tests are the point-of-care alternative to gold standard RT-PCR, for frequent and affordable testing. Rapid antigen tests can screen for current infection at the point of care (POC),[3] and are used to identify and isolate infected people as early as possible to control the transmission, but typically suffer from inadequate sensitivity.[4,5] Serology tests detect the presence of host antibodies arising from past infection (or vaccination), useful in assessing individual and population immunity, though not standard practice for detection of active infection.[6] Technologies for POC molecular tests are emerging but currently there are only a limited number of field-ready devices and these are cost-prohibitive for frequent testing.[7] Thus, there remains a need for sensitive, cost-effective detection formats for frequent use at the point of care.

Advancements in sample collection, assay chemistry, isothermal nucleic acid amplification techniques, CRISPR-based workflows, microfluidics, test architecture, materials and instrumentation have been implemented to enhance the sensitivity of point of care detection technologies, mainly of lateral flow immunoassays (LFAs).[8] LFAs continue to be the preferred format for POC diagnostics because they are rapid, affordable, and user-friendly.[7,9] LFAs are based on capillary wicking of a liquid sample along a nitrocellulose membrane bearing immobilized (capture) antibodies on test and control lines. As the sample wicks through the membrane, it contacts reporter particles decorated with antibodies to the target. The particle-antibody-target complexes are captured by the anti-target antibodies immobilized on the test line, and particles are captured independent of the target on the control line, resulting in the lines characteristic of a positive LFA. LFAs are used in a wide array of diagnostic applications including screening for respiratory infections, *e.g.* flu and COVID-19. However, LFAs very often suffer from limited clinical sensitivity when validated at POC with clinical samples. Currently, despite the self-reported high sensitivities of several commercially available SARS-CoV-2 rapid antigen tests, there are several published reports of poor performance (and significantly lower sensitivities than initially reported), especially when used in asymptomatic patients in

[a]*Department of Biomedical Engineering, University of Houston, Houston, Texas 77204, USA. E-mail: willson@uh.edu*
[b]*Department of Chemical and Biomolecular Engineering, University of Houston, Houston, Texas 77204, USA. E-mail: jcconrad@uh.edu, edkourentzi@uh.edu*
[c]*Department of Biology and Biochemistry, University of Houston, Houston, Texas 77204, USA*
[d]*Escuela de Medicina y Ciencias de Salud, Tecnológico de Monterrey, Monterrey, Nuevo León 64710, Mexico*

†Electronic supplementary information (ESI) available. See DOI: **https://doi.org/10.1039/d2an01499h**

‡Present address: Merck, Kenilworth, New Jersey 07033, USA.
§Present address: Purification Process Sciences, BioPharmaceuticals Development, R&D, AstraZeneca, Gaithersburg, Maryland 20878, USA.

low prevalence settings or by non-trained users.[4,5,10] Thus, there is still a need for technologies that could enable user-friendly LFAs of increased sensitivity that are compatible with clinical samples.

The analytical sensitivity of LFAs, given high-performance antibodies, can be enhanced with the use of reporter particles of increased detectability.[9,11] Conventional gold and latex colorimetric reporters report the presence of a pathogen by visible lines but typically have limited analytical sensitivity.[8] Higher-sensitivity reporters include organic fluors,[12] europium chelates,[13,14] quantum dots,[15,16] up-converting nanoparticles,[17] enzyme-mimicking, metal catalytic nanoparticles,[18,19] SERS-active nanomaterials,[20] and paramagnetic nanoparticles.[21] These reporters can greatly enhance LFA sensitivity but typically require custom synthesis protocols or costly and/or complex readers.[22] Achieving high analytical sensitivity without sacrificing the simplicity and low cost of LFA remains an open challenge.

We previously introduced filamentous, nonspherical M13 bacteriophage particles as LFA reporters combining enhanced detectability and capturability.[23–28] We also identified (through detailed mechanistic studies) their anisotropic shape as a source of their improved performance in LFA.[26–28] Moreover, M13 phage are stable, non-hazardous, monodisperse, neutrally buoyant, under Darwinian selection for non-aggregation and low nonspecific stickiness, well-characterized, commercially available, cheap, and easy to produce in large quantities.[29] M13 phage possess a high surface area/volume ratio and the abundant M13 phage coat proteins can be exploited to attach multiple copies of recognition elements, *e.g.* antibodies or aptamers, and reporter enzymes (*e.g.* horseradish peroxidase (HRP)) or fluors for signal amplification through different bioconjugation strategies.[30] These phage reporters exhibited extremely low limits of detection in model systems or using sophisticated fluorescence instrumentation in mechanistic investigations of LFAs,[23–28] but were not tested on real samples at the point of care.

In this study we demonstrate a novel platform technology for highly sensitive rapid POC immunoassays, LFAs employing M13 phage-based chemiluminescent reporters, read by a smartphone, and compatible with clinical samples. For the initial validation of the technology, we demonstrate the ultrasensitive detection of SARS-CoV-2 nucleoprotein in nasal swab extracts using an off-the-shelf smartphone (fitted with a $1.20 3-D printed accessory) and an in-house developed iOS app for imaging and analysis. Moreover, we report fully-detailed protocols for antibody screening and conjugation chemistries, the coordinates for the inexpensive smartphone reader accessory and a rational workflow for assay development to enable broad adoption of M13 phage LFAs by others in the field.

2. Materials and methods

2.1. Materials

Hydroxylamine hydrochloride (99%), sodium *meta*-periodate (≥99%), IGEPAL CA-630, bovine serum albumin (A7906, ≥98%), polyvinylpyrrolidone (PVP-40, average MW 40 000), and sodium acetate (99%) were purchased from Sigma Aldrich and used without modification or purification. Sodium carbonate was from Millipore Sigma. Sodium cyanoborohydride was purchased from CHEM-IMPEX and used without modification. Phosphate-buffered saline (PBS) tablets were from TaKaRa. Enhanced Chemiluminescence (ECL) Ultra substrate (acridan-based; TMA-6) was purchased from Lumigen and 1-Step Ultra TMB-ELISA Substrate Solution was from Thermo Scientific.

2.2. Nasal swab samples

For spiking studies, fresh presumed-negative anterior nasal swab specimens were self-collected by adult lab members under a University of Houston IRB-approved study (UH STUDY00002547) using Puritan foam tip swabs. Each swab was extracted with 1 mL of LFA extraction buffer (1× PBS (pH 7.4), 10 mg mL^{-1} BSA, 5 mg mL^{-1} PVP-40, and 0.25% v/v IGEPAL CA-630), for at least 2 min, and then the swab was discarded. Nasal swab extract samples were used immediately.

To test the compatibility of phage LFA with clinical samples, we initially used frozen, de-identified post-diagnostic molecular testing, nasopharyngeal swab extracts, a generous gift from University of Texas Medical Branch at Galveston (Dr Scott Weaver and Ms Nehad Saada) and Community Labs, LLC (Dr Scott Jones). Frozen, de-identified, anterior nasal swabs extracted in saline (leftovers from diagnostic molecular testing with known Ct values, but unknown stage of disease) were purchased from Labcorp. Such leftover clinical samples are typically used in the initial evaluation of a test under development when available and affordable to purchase.[5,31,32] Studies with these de-identified clinical specimens were not considered human subjects research. Handling and testing of clinical specimens were performed under BSL-2 containment inside a Nuaire Class II Biological Safety Cabinet (UH MUA #008-20).

2.3. LFA phage reporters

IgG–horseradish peroxidase (HRP)-conjugates (Peroxidase AffiniPure Goat Anti-Mouse IgG, Jackson ImmunoResearch, 115-035-003) were treated with periodate to oxidize the oligosaccharide residues of IgG Fc and HRP and create amine-reactive aldehyde groups.[33] These aldehydes were then conjugated to the exposed primary amines of M13mp18 phage (Guild Biosciences; M13mp18 is a commercially available and well-characterized engineered derivative of wild-type M13 bearing the same coat proteins as the wild-type) proteins *via* reductive amination. Briefly, 0.1 M sodium *meta*-periodate and goat anti-mouse antibody–HRP conjugates were mixed in 100 mM sodium acetate, pH 5.5, to final concentrations of 1.68 mg mL^{-1} and 0.22 mg mL^{-1}, respectively, and allowed to react at room temperature for 20 min. Unreacted periodate was removed using a Zeba Spin Desalting Column 7K MWCO (Thermo Fisher Scientific), pre-equilibrated with 200 mM sodium carbonate, pH 9.6. 100 μL of M13 phage (9×10^{13} virions per mL) in 200 mM sodium carbonate, pH 9.6, was added to the oxidized antibody/HRP conjugates (estimated 30

antibody/HRP conjugates offered per phage) and allowed to react for 2.5 h at room temperature. Sodium cyanoborohydride (4 μL of 5 M in 1 M sodium hydroxide) was added to the reaction (400 μL) to a final concentration of 0.05 M to reduce the unstable Schiff bases formed by the reaction of primary amines and aldehydes to stable secondary amines, and the mixture was incubated for 30 min at room temperature. Next, hydroxylamine hydrochloride (1 M in DI water) was added to a final concentration of 0.05 M to quench the reaction and the resulting solution was incubated for 30 min at room temperature. Uncoupled antibodies were removed by passing the solution through a Capto Core 700 resin (Cytiva) column (2 mL) pre-equilibrated with 1× phosphate-buffered saline solution (PBS).[34] Phage construct concentration was determined using UV-Vis absorbance (Thermo NanoDrop ND-1000 UV/Vis Spectrophotometer) and the formula: virions per mL = $[(A_{269nm} - A_{320nm}) \times 6 \times 10^{16}]$/genome length[35] (7249 nt for M13mp18). Phage constructs were stored in 1× PBS at 4 °C until use. Prior to functional testing in phage LFA, the apparent enzymatic activity of the phage conjugate was confirmed in solution against a calibration curve of unmodified HRP enzyme using the 1-Step Ultra TMB HRP substrate in a 96-well microtiter plate, with absorbance at 450 nm measured by a TECAN Infinite M200 PRO plate reader.

2.4. LFA assembly and antibody striping

A 25 mm wide by 300 mm long UniSart CN140 nitrocellulose membrane (Sartorius Stedim) and a 22 mm ReliaFlow™ 440 absorbent pad (Ahlstrom-Munksjö) were placed on a 300 mm long backing card (DCN, MIBA-020) with a 2 mm overlap. 1 mg mL^{-1} rabbit monoclonal anti-SARS-CoV-2 nucleoprotein antibodies and 0.5 mg mL^{-1} goat polyclonal anti-mouse antibodies (Arista Biologicals, ABGAM-0500) in 1× PBS were dispensed on the membrane using a Biodot XYZ3060 system (flow rate 1 μL cm^{-1}) to form test and control lines, respectively. The membranes were allowed to dry at 50 °C for 1 h and stored in a desiccator overnight. The membranes were cut into 3 mm wide strips using a ZQ2000 Guillotine Cutter (Kinbio Tech) and stored desiccated at room temperature until use.

2.5. LFA running protocol

Based on previous experience and a brief screening, the formulation of the LFA running/extraction buffer used in this work was 1× PBS (pH 7.4), 10 mg mL^{-1} BSA (blocking/passivation agent), 5 mg mL^{-1} PVP-40 (a neutral polymer to facilitate dispersion), and 0.25% v/v IGEPAL CA-630 (a nonionic, non-denaturing immunoassay-compatible surfactant commonly used for virus lysis).

Recombinant SARS-CoV-2 nucleoprotein (ACRO Biosystems, NUN-C5227; calculated MW 47.3 kDa; GenBank: QHO62115.1) in extraction buffer or negative nasal swab extract (24 μL) was mixed with 6 μL of 2 μg mL^{-1} mouse anti-nucleoprotein antibodies (final concentration of 0.4 μg mL^{-1} antibody in 30 μL sample). Half-strip LFA was dipped into 30 μL of the sample followed by 10 μL of reporter phage conjugates (3×10^{11} virions per mL in extraction buffer) followed by three washes with 10 μL of the extraction buffer. Finally, 20 μL of Enhanced Chemiluminescence (ECL) substrate for HRP was applied to each strip by pipetting directly over the test and control lines and the strip was imaged as described below.

2.6. Imaging and analysis

LFA strips were imaged both with a laboratory imager and a smartphone. For test optimization/development, LFA strips were imaged using an Alpha Innotech FluorChem gel documentation system equipped with a CoolSNAP K4 CCD camera (no filters; exposure time: 3 s, binning: 4; pixel size: 7.4 μm), immediately after substrate application. Images were captured at 3 s time intervals for at least 7 min. Intensity profiles were extracted from the images using the plot profile tool of NIH ImageJ.[36] A horizontal line was drawn along the baseline in the intensity profiles and the areas under the peaks were selected and measured using the ImageJ measure tool. These values were the intensities of the control (CL) and test line (TL) (Fig. S1 in the ESI†). The TL/CL ratio reached its maximum 6 min after adding the substrate and this time (noted by the vertical dashed line in Fig. S2 in the ESI†) was chosen for all the LFA strips imaged on the FluorChem system (Fig. S2†).

The applicability of the phage LFA for point-of-care use was demonstrated using an iPhone XR fitted with a 3-D printed lens-free accessory (Fig. S3 in the ESI;† in-house designed and made available at Thingiverse; **https://www.thingiverse.com/thing:5178342**) to properly position the strip directly under the (more light sensitive) back camera. A custom iOS app (originally developed and used by courtesy of Glow Nanotech, LLC) was employed for image analysis. The app reads the LFA strip by acquiring 10 images in RAW format with predefined parameters (no flash, ISO: 2500, focus: 0, exposure: 1000 ms, pixel size: 1.4 μm). The intensity values of blue pixels (chosen because the peak intensity of ECL light emission occurs at 440 nm) from the region of interest of each image were extracted and averaged across the strip width to generate ten 1-D intensity profile arrays. To further reduce the sensor noise, the ten intensity profile arrays were averaged together into one intensity profile array. The app then determined the location of the control line (CL) by identifying the pixel with maximum intensity in the top half of the LFA strip, downstream from the test line. Next, the app validated the CL by checking the maximum intensity against a preset threshold (twice the intensity profile minimum). The CL served as the reference point to locate the test line (TL), a local maximum at 400 ± 75 pixels away (5 mm). The background (BG) was determined midway between the CL and TL by finding the local minimum at 200 ± 75 pixels away from the CL peak. The integrated intensity values of CL, TL, and BG were calculated using the trapezoidal rule with lower and upper integrating limits of peak location ±25 pixels. Finally, the value of TL/CL ratio was determined as TL/CL = (TL − BG)/(CL − BG). In preliminary experiments, we observed that the TL/CL ratio reached its maximum value 3 min after adding the substrate and this time was used for all smartphone measurements (Fig. S4 in the ESI†). We attribute the difference in the smartphone-based analysis time (3 min

as compared to 6 min with the FluorChem System) to the fact that the strip was tightly constrained inside a plastic LFA cassette (Fig. S3 in the ESI†) and its side walls accelerated the flow and penetration of the HRP substrate through the nitrocellulose.

2.7. Antibody screening in LFA

Twelve capture antibodies (rabbit monoclonal anti-SARS-CoV-2 nucleoprotein antibodies) and seven detection antibodies (mouse monoclonal anti-SARS-CoV-2 nucleoprotein antibodies) (Table 1) were screened in all possible combinations directly on LFA half-strips. Each pair was initially tested with a no-analyte (negative) sample and 5 ng mL^{-1} SARS-CoV-2 recombinant nucleoprotein (ACRO Biosystems, NUN-C5227) in LFA extraction buffer using anti-mouse IgG/HRP phage reporters. Pairs were ranked based on the difference between the TL/CL ratios of positive (specific signal) and negative (nonspecific signal) strips. In the second round of screening, antibody pairs were tested with a no-analyte and 1 ng mL^{-1} of nucleoprotein in extraction buffer. The third round of screening was performed using nasal swab extract spiked with serial dilutions of nucleoprotein. Antibody screening was performed with a consistent initial protocol and a single batch of phage reporters and LFA strips for objective comparison of antibodies.

2.8. RT-qPCR testing

We adapted the Yale SalivaDirect RT-PCR assay[37] for use with nasal swab extracts. Nasal extract (50 μL) was first treated with proteinase K (6.3 μL of 20 mg mL^{-1}) by vortexing for 1 min (Vortex Genie 2, analog control knob at 7) followed by heat inactivation (95 °C, 5 min) and 5 μL used as input in singleplex RT-qPCR reactions using the CDC 2019-nCoV-2 RUO premixed primer and probe sets (IDT DNA Technologies; N1 and RP) and the Luna Universal Probe One-Step RT-qPCR Kit (E3006S; New England Biolabs) on an MX3005P qPCR instrument (Agilent). For each singleplex RT-qPCR reaction, 5 μL of processed sample was mixed with 1.5 μL of primer/probe mixture (final primer and FAM/BHQ-1-probe concentrations were 500 nM and 125 nM, respectively), 1 μL of 10× Luna WarmStart® RT Enzyme Mix, 10 μL of 2× Luna Universal Probe One-Step Reaction Mix, and 2.5 μL of nuclease-free water. The RT-PCR conditions were 10 min at 52 °C (Reverse Transcription/cDNA synthesis step), 2 min at 95 °C, and 45 cycles of 10 s at 95 °C and 30 s at 55 °C. Dilutions of SARS-CoV-2 (2019-nCoV) RUO plasmid control containing the nCoV nucleoprotein gene (GenBank NC045512.2; IDT DNA Technologies; 5×10^5 to 50 copies per reaction) in nuclease-free water were used to construct standard curves for every run (typical observed amplification efficiency of 0.91). To confirm the input of human RNA the Hs_RPP30 plasmid control (IDT DNA) was used, which contained a portion of the single copy, human ribonuclease P protein subunit p30 gene. Control reactions in which no template was included (termed "no template control" (NTC) negative reactions) did not exhibit amplification curves that crossed the threshold line and thus no Ct value was reported. qPCR Control SARS-CoV-2 RNA (BEI NR-52347) was used as a positive control (1250 genome equivalents per 5 μL, Ct value 26.6 ± 0.7, $n = 4$).

Table 1 Commercial anti-SARS-CoV-2 nucleoprotein monoclonal antibodies were screened in the phage LFA. Final selected antibodies (capture: #3 and detection: #12) are highlighted in gray

Index	Vendor	Catalog #
1	Bioss Antibodies	m-bsm-41411M
2	Ray Biotech	5F7B3
3	Ray Biotech	1G1-F2
4	Ray Biotech	1A4g1G12G12
5	Pro Sci	35720
6	Sino Biological	40143-MM08
7	Sino Biological	40143-MM05
8	ExonBio	NP11A7
9	ExonBio	NP5B1
10	ExonBio	NP5E2
11	ExonBio	NP11H9
12	ExonBio	12F1
13	ExonBio	NP12C1
14	ExonBio	NP12E6
15	ExonBio	NP12B8
16	Ray Biotech	130-10760
17	Pro Sci	10-352
18	Sino Biological	40143-R004
19	ExonBio	NP12A1

2.9. Clinical sensitivity with banked samples

De-identified, anterior nasal swab liquid samples including 12 negative and 15 positive samples were tested in phage LFA. To condition the sample while minimizing analyte dilution, clinical samples were mixed 4 : 1 with 6 μL of 2 μg mL^{-1} mouse anti-nucleoprotein antibodies in 5× concentrated extraction buffer to leave the samples in 1× LFA extraction buffer and 0.4 μg mL^{-1} detection antibodies (mouse anti-nucleoprotein antibodies). 30 μL of this sample was run on an LFA strip followed by anti-mouse IgG/HRP phage reporters and the rest of the protocol was as described in Section 2.5.

IBM SPSS statistics software 28.0.1.0 (IBM, Armonk, NY) was used to run Mann–Whitney U tests and the receiver operating characteristic (ROC) curve analyses.

3. Results and discussion

3.1. Universal antibody-enzyme phage LFA reporters

We chemically functionalized M13 phage proteins with anti-mouse IgG/HRP conjugates by oxidation of polysaccharides on antibodies and HRP enzymes to make universal, easily-customizable ultrasensitive LFA reporters. The sample was mixed with mouse monoclonal anti-nucleoprotein detection antibodies, and as the sample migrated into the nitrocellulose membrane, detection antibody–analyte complexes were captured on the test line bearing rabbit monoclonal anti-nucleoprotein antibodies. The unbound antibodies were captured by anti-mouse antibodies on the control line. Anti-mouse antibody/HRP phage reporters were then added, and HRP cap-

tured on the test line and control line oxidized luminol in the chemiluminescent substrate, which generated a light signal readily detectable by an unmodified smartphone (Fig. 1).

We chose to target the viral nucleoprotein (N protein). The nucleoprotein is a highly conserved and abundantly expressed viral structural protein in SARS-CoV-2 [38] and becomes accessible after a simple detergent-based sample treatment. Thus, it is the preferred diagnostic target (over the mutation-prone surface trimer spike protein)[39] and the majority of the SARS-CoV-2 antigen tests under FDA EUA target the nucleoprotein.[40]

We initially investigated different strategies for the direct conjugation of anti-nucleoprotein antibodies and HRP enzymes on the primary amines of the phage proteins,[41] including the commonly-used carbodiimide-mediated crosslinking with EDC and sulfo-NHS, Traut's reagent thiolation of primary amines for coupling to maleimide-activated antibodies,[23,24] and periodate-mediated oxidation of glycosylated antibody Fc and HRP sugars to amine-reactive aldehydes. All antibody–HRP phage conjugates tested performed well in ELISA and were captured on LFA control lines but the signal for nucleoprotein on test line was not detectable. Phage functionalized with commercial (pre-conjugated) anti-mouse IgG/HRP conjugates combined with soluble mouse anti-nucleoprotein antibodies, however, showed superior LFA analytical sensitivity.

3.2. Antibody screening

The performance of immunoassays depends critically upon the pair of antibodies used. Traditional equilibrium-based antibody screening methods such as ELISA, however, are not predictive of the behavior of antibodies when integrated in LFA format.[42,43] Thus, we performed three rounds of antibody screening directly in phage LFA. First, we screened all 84 monoclonal antibody pairs against SARS-CoV-2 nucleoprotein (Table 1) in phage LFA using a negative (0 ng mL^{-1}) and a high positive (5 ng mL^{-1} nucleoprotein) sample in extraction buffer (Fig. 2). We calculated the ratio of the intensities of test and control lines and ranked the pairs based on the difference between the ratio of test line to control line of positive strips and negative strips $(TL/CL)_{positive} - (TL/CL)_{negative}$ for each pair (Fig. 2). Interestingly, seven antibody pairs demonstrated nonspecific signal (negative strip) that was greater than the specific signal (positive strip) whereas eighteen pairs demonstrated indistinguishable nonspecific and specific signals. The six antibody pairs with the highest ranking and in sufficient stock (shown in bold in Fig. 2) were then tested with 1 ng mL^{-1} nucleoprotein in LFA extraction buffer. The differences between the TL/CL values of positive strips and negative strips ($(TL/CL)_{positive} - (TL/CL)_{negative}$) for the six pairs were: 8-3: 0.22, 9-3: 0.08, 10-3: 0.11, 12-3: 0.34, 13-3: 0.32, 14-3: 0.34. The two antibody pairs with the highest ranking and in sufficient stock, 13-3 and 12-3, were then tested with nucleoprotein (0, 0.05, 0.1, and 0.5 ng mL^{-1}) spiked in nasal swab extract. The difference in TL/CL of negative strips and low positive strips (0.05 ng mL^{-1}) was higher for the 12-3 pair (Fig. S5 in the ESI†). Consequently, we used this pair, #12, rabbit monoclonal antibody 12F1 (ExonBio) and #3, mouse monoclonal antibody

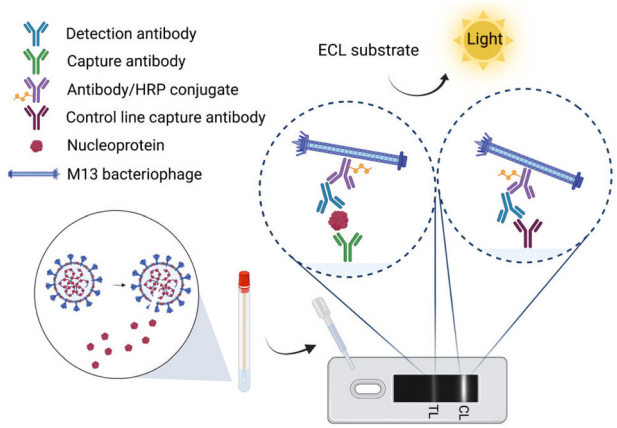

Fig. 1 Schematic illustration of the chemiluminescent phage lateral flow assay for the detection of SARS-CoV-2 nucleoprotein. The sample flows along a nitrocellulose membrane on which immobilized (rabbit) antibodies capture the nucleoprotein molecules on the LFA test line (TL). Murine detection antibodies bind to the captured nucleoprotein molecules and are then detected by anti-mouse antibody–HRP M13 phage reporters. Light signal from the HRP-mediated chemiluminescent reaction is captured and analyzed by a smartphone and associated app. Created with BioRender.com.

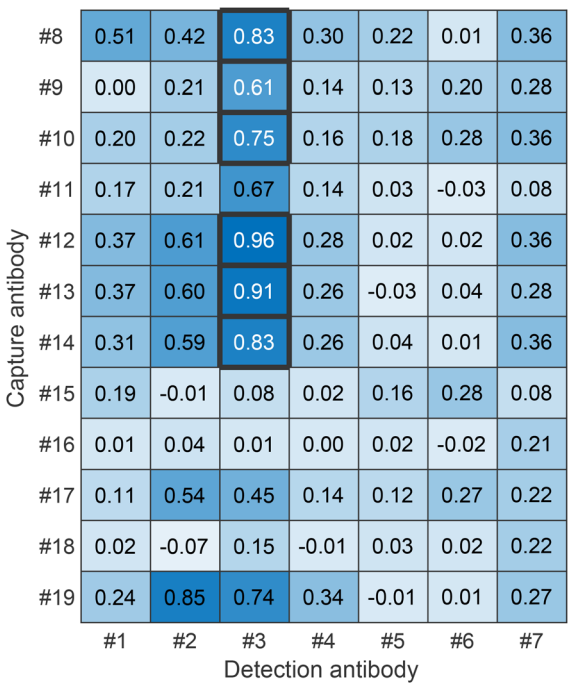

Fig. 2 Phage LFA-based antibody screening. The performance of the 84 antibody pairs was initially evaluated with a no-target and 5 ng mL^{-1} nucleoprotein sample in LFA extraction buffer. Values shown are the differences between the TL/CL ratios of positive and negative strips; darker blues correspond to higher differences. The top 6 antibody pairs that were available in sufficient stock (shown in bold borders) were chosen for the next round of screening using 1 ng mL^{-1} nucleoprotein.

1G1-F2 (Ray Biotech), for further test development and validation.

Given the proof-of-concept nature of the study, we did not perform any antibody cross-reactivity studies. Based on available wet testing of other anti-SARS-CoV-2 antibodies and *in silico* analyses of different pathogens (comparing sequence homology on NCBI BLAST) as presented in the documents of FDA EUA-authorized tests,[40] antibodies raised against SARS-CoV-2 have been found to be not cross-reactive with a large number of commensal and pathogenic microorganisms expected to be found in respiratory samples. It is a common expectation that these antibodies would cross-react with SARS-CoV nucleoprotein, but this has not been deemed as a significant limitation since co-circulation of those two coronaviruses is highly unlikely.

3.3. Analytical sensitivity with contrived samples

Following antibody screening we evaluated the analytical sensitivity of the chosen antibody pair in phage LFA with nasal swab extracts (presumed-negative for COVID-19) spiked with recombinant nucleoprotein (25 pg mL^{-1} to 500 pg mL^{-1}; Fig. 3). The signal increased linearly with increasing nucleoprotein concentration and the limit of detection (LoD), defined as the lowest analyte concentration for which the signal is above the $average_{blank} + 3 \times STD_{blank}$, was 25 pg mL^{-1} (0.53 pM). There is no general consensus on the required analytical sensitivity to ensure clinical utility. A recent study[44] using the Quanterix SIMOA technology showed a median nucleoprotein concentration of 215 pg mL^{-1} in PCR-positive banked swabs (n = 148 with 71 samples with ≥1000 pg mL^{-1}). Thus the sub-picomolar LoD of the phage LFA in nasal swab extract is promising and better than the LoD in recently reported SARS-CoV-2 nucleoprotein colorimetric LFAs, as discussed in Section 3.5.

3.4. Clinical sensitivity with nasal swab extracts

Here, we adapted the Yale SalivaDirect assay that circumvents RNA extraction and performed RT-PCR directly on nasal swab extracts. We obtained Ct values for Labcorp positive samples (received frozen and then thawed) that were an average 1.9 (±2.3) cycles higher than the Labcorp-supplied Ct values (with a Spearman's correlation coefficient of 0.89) demonstrating that our direct RT-PCR was sufficient for the needs of our study (to benchmark serially-diluted pooled samples prior to LFA testing during LFA optimization and for periodically checking fresh nasal specimens). All Labcorp negative samples gave Ct values greater than 40.

We tested 27 de-identified nasal swab extracts from Labcorp, including 15 positive samples with known Ct values ranging from 18.7 to 29.6 (3 samples with Ct values greater than 28) and 12 negative samples (Ct values not reported but greater than 40) (Table S1 in the ESI†). The LFA signals for PCR-positive samples were statistically different from the negative samples (Mann–Whitney U test, $p < 0.001$; Fig. 4; Fig. S6 in the ESI:† LFA signal and Ct value for all positive samples tested) indicating that phage LFA was sufficiently sensitive to

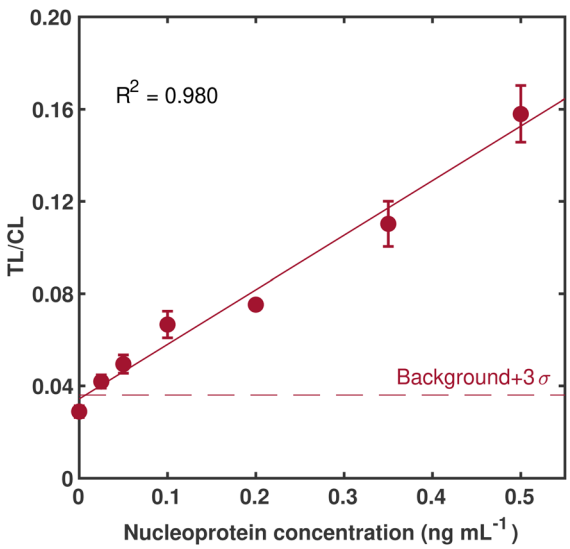

Fig. 3 Sub-picomolar (25 pg mL^{-1} = 0.53 pM) detection of nucleoprotein in nasal swab extract using the phage LFA. Nucleoprotein was spiked in presumed-negative fresh nasal swab extracts; capture: rabbit monoclonal antibody 12F1 (#12) ExonBio and detection: mouse monoclonal antibody 1G1-F2 (#3) Ray Biotech. LFA strips were imaged 6 minutes after adding the ECL substrate, on a FluorChem gel documentation system. Data are mean ± s.d.; the experiments were repeated at least three times. The dashed red line denotes the estimated background as the average plus three times the standard deviation ($\mu + 3\sigma$) of the negative tests.

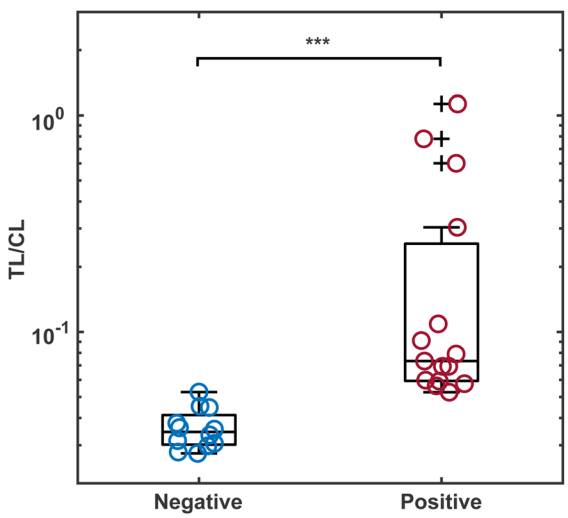

Fig. 4 Individual results of clinical specimens (nasal swab extracts from Labcorp) tested using the phage LFA and read with lab instrumentation. The box plots display the phage LFA TL/CL ratios of negative (n = 12) and positive samples (n = 15). Horizontal lines on each box plot, from bottom to top beginning with the bottom whisker are: 10th percentile, 25th percentile, median, 75th percentile, and 90th percentile. + symbols indicate outliers (low Ct value samples, 21.1, 19.5 and 18.7). *** symbol indicates that the two groups are statistically different by the Mann–Whitney U test, $p < 0.001$. TL/CL as a function of Ct value is shown in Fig. S6 in the ESI.†

discriminate between positive and negative samples. We carried out ROC analysis (albeit with a very limited number of samples, shown in Fig. S7 in the ESI†), and demonstrated a maximum sensitivity of 93.3% at 100% specificity (area under the ROC curve (AUC) = 0.994; 95% CI 0.977–1.00). We note, however, that significantly more samples are required to formally assess the clinical performance of the technology. The inherent variability of the human matrix is evident from the observed range of the background values of the negative human samples (and the background value of the fresh samples; Fig. 3). This variation could affect the estimated cutoff value and thus the analytical sensitivity as estimated in Fig. 3. Ultimately, fresh clinical specimens are required to predict the clinical potential of the immunoassay in the "real world". Further optimization of the extraction reagent/diluent and LFA materials may be needed to contend with the viscosity and variable nature of fresh clinical samples. Nonetheless, the phage LFA was sufficiently sensitive to discriminate between positive and negative clinical samples (Fig. 4), despite the inherent variability in nasal swab background. We note that recent studies have tried to correlate the performance of LFA with PCR Ct values[45–47] but differently-calibrated PCR systems, different workflows, and fundamentally different targets (nucleic acid *vs.* protein) hinder the drawing of general conclusions.

3.5. Smartphone-based phage LFA

Smartphones provide a now-ubiquitous, portable, and user-friendly platform to image and interpret optically-reporting LFAs.[48] Moreover, the wavelength of the ECL chemiluminescent emission matches the smartphone camera spectral sensitivity curve.[49,50] We developed a 3D-printed attachment that positions the LFA strip directly under the back camera of the iPhone XR and blocks out all ambient light, maintaining a dark environment (Fig. S3 in the ESI†). An iOS image analysis app was developed in-house (a typical analysis screenshot is shown in Fig. S3†).

We tested nucleoprotein serially diluted in nasal swab extract and read the LFA strips using the iPhone reader. The TL/CL ratio increased with increasing nucleoprotein concentration (Fig. 5) and the LoD was estimated at 100 pg mL^{-1}. The smartphone-based LoD value was higher than the LoD estimated using the CCD camera of the bulkier and more expensive FluorChem imaging system. Nevertheless, the off-the-shelf, portable and affordable smartphone reader showed a low and clinically-relevant[44] LoD in addition to the user-friendly and point-of-care features of the smartphone platform.

We have compared the LoD of recently published, state-of-the-art SARS-CoV-2 antigen LFAs in Table S2 (ESI; page S9†). Despite the complex and inherently variable nature of human nasal samples, the LoD of the phage LFA is better than most recently reported values (for the detection of SARS-CoV-2 nucleoprotein or spike protein) in equipment-free colorimetric LFAs (gold nanoparticles,[51–53] latex particles,[54] cellulose nanobeads;[55,56] Table S2 in the ESI†). The analytical sensitivity of phage LFA is even comparable to that of fluorescent LFAs read by costly and specialized readers[15,16] and that of a nanozyme-based LFA (imaged by a smartphone but image analysis done using a computer (LoD determined in buffer)).[57]

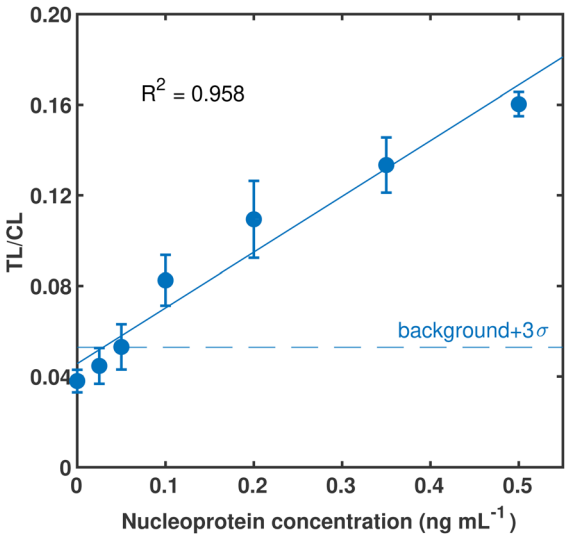

Fig. 5 Smartphone-based picomolar detection of nucleoprotein using the phage LFA. Nucleoprotein was spiked in presumed-negative nasal swab extracts; capture: rabbit monoclonal antibody 12F1 (#12); ExonBio and detection: mouse monoclonal antibody 1G1-F2 (#3); Ray Biotech. Data are mean ± s.d.; n = 3. The dashed blue line denotes the estimated background as the average plus three times the standard deviation (μ + 3σ) of the negative tests.

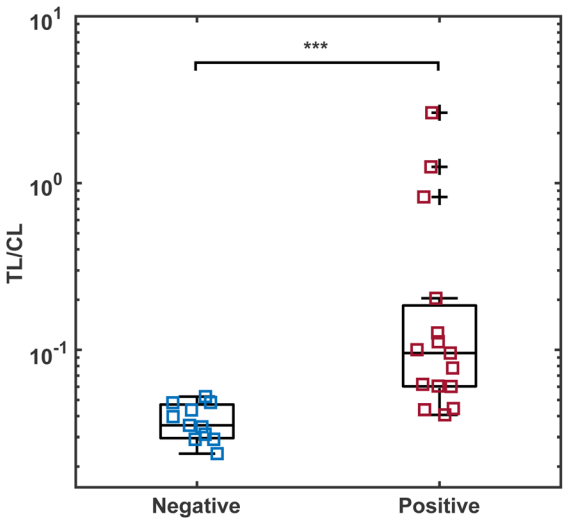

Fig. 6 Individual results of clinical specimens (nasal swab extracts from Labcorp) tested using the phage LFA read with a smartphone. The box plots display the LFA signals (TL/CL) of negative (n = 11) and positive samples (n = 15). One negative sample used in the experiments presented in Fig. 4 was exhausted before testing with smartphone imaging and analysis. Horizontal lines on each box plot, from bottom to top beginning with the bottom whisker are: 10th percentile, 25th percentile, median, 75th percentile, and 90th percentile. + symbols indicate outliers (low Ct value samples, 21.1, 19.5 and 18.7). *** symbol indicates that the two groups are statistically different by the Mann–Whitney U test, p < 0.001. TL/CL as a function of Ct value is shown in Fig. S8 in the ESI.†

Post-LFA signal amplification (*e.g.* with copper deposition on gold nanoparticles[58]) was shown to greatly improve the LoD of gold LFAs, but at the expense of increased background that may hinder reliable visual interpretation, simplicity or economy. Other enhancement strategies, *e.g.* thermal contrast amplification on gold nanoparticles,[59] may hinder POC applicability since the enhanced LFA strip is read with complex equipment.

Next, we tested 26 nasal swab clinical samples including 15 positive and 11 negative samples, in phage LFA and read and analyzed the signals using the smartphone (Fig. 6; Fig. S8 in the ESI:† LFA signal and Ct value for all positive samples tested). Using a Mann–Whitney *U* test, negative samples tested and positive samples tested were confirmed to be statistically different ($p < 0.001$) indicating that the smartphone-read phage LFA was sufficiently sensitive to discriminate between positive and negative clinical samples. We reached a maximum sensitivity of 80% at 100% specificity (area under the ROC curve (AUC) = 0.939; 95% CI 0.854–1.00) based on the ROC analysis (ROC curve with a very limited number of samples is shown in Fig. S9 in the ESI†). However, significantly more samples would be required to reliably assess the clinical performance of the technology.

4. Conclusions

We engineered a new, universal class of LFA reporters by conjugating nonspherical M13 phage with anti-mouse IgG/HRP conjugates and demonstrated a translation-ready, ultrasensitive phage LFA platform technology. The transition to anisotropic, soft-material LFA reporters as opposed to conventional spherical gold particles will lead to LFAs with enhanced analytical sensitivity and enable rationally-engineered LFAs. Initial validation of the technology was demonstrated in the point-of-care detection of SARS-CoV-2 nucleoprotein in clinical samples. By combining the advantages of anisotropic phage reporters and enzyme-generated chemiluminescence, we demonstrated an LoD of 100 pg mL^{-1} for SARS-CoV-2 nucleoprotein spiked in nasal extract read by an off-the-shelf smartphone. The LoD of the phage LFA is better than most of the best visual LFAs and even comparable to LFAs read by specialized readers (Table S2 in ESI; page S9†). Furthermore, the phage LFA was demonstrated to overcome the challenge of testing human clinical samples, achieving excellent clinical sensitivity with 15 banked PCR-confirmed positive nasal swab extracts of Ct values between 18.7 to 29.6 and 11 negative samples (several of the high-sensitivity LFAs have not been validated with real clinical samples, Table S2†).

Further improvements in the smartphone reader, *e.g.* by the addition of a macro lens for light focusing (increasing the accessory cost by $3 to $5; cost amortized over numerous tests) could enhance detection sensitivity without increasing the test complexity for the end user. Recent advances in device[60] engineering and materials[61] such as custom-made LFA cassettes to accommodate pre-storage of the lyophylized substrate and automatic rehydration and release or larger volumes of liquids, could facilitate the integration of chemiluminescence into user-friendly, point-of-care diagnostics.

Beyond COVID-19 diagnostics, the phage LFA platform technology has very broad potential applications, including the detection of infectious disease agents, food toxins, and environmental contaminants at point of care/need. Our smartphone-readable phage LFA reporters would enable lateral flow tests that are rapid, ultrasensitive, user-friendly, equipment-free, low-cost, and potentially rapidly widely deployable, thereby enabling large-scale diagnostic testing of diseases and infections that need emergency response or at-home medical testing.

Author contributions

M. C. performed the experiments and analyzed the data. B. V., K. B., and M. S. helped with running the experiments and data analysis. D. C. and K. K. ran the qPCR experiments; K. K., J. C. C., and R. C. W. designed and advised the project. K. K., M. C., J. C. C., and R. C. W. wrote and edited the manuscript, and all authors provided feedback.

Conflicts of interest

Authors Binh Vu and Richard C. Willson are named inventors on IP which could relate to the subject of this paper.

Acknowledgements

We gratefully acknowledge Dr Scott Weaver and Ms Nehad Saada at University of Texas Medical Branch at Galveston and Dr Scott Jones at Community Labs, LLC (San Antonio, TX) for the de-identified clinical samples used in preliminary studies. We thank Krisha Doshi at ExonBio and Lawrence Gray at IDT for helpful discussions. The following reagent was deposited by the Centers for Disease Control and Prevention and obtained through BEI Resources, NIAID, NIH: Quantitative PCR (qPCR) Control RNA from Heat-Inactivated SARS-Related Coronavirus 2, Isolate USA-WA1/2020, NR-52347. We gratefully acknowledge financial support from the University of Houston "Grants to Enhance Research on COVID-19 and the Pandemic" Program (Grant #000180936 and Grant #00180943), the NIH Rapid Acceleration of Diagnostics (RADx) Program, NIH/NIAMS (Grant #1R01AR072742-01), NIH/NIAID (Grant #1R61AI174294-01), DOD CDMRP (Grant #W81XWH-21-1-0975), the National Science Foundation (CBET-1803728 and CBET-1928334), and the Welch Foundation (E-1869).

Notes and references

1 S. Das and S. Dunbar, *Front. Cell. Infect. Microbiol.*, 2022, **12**, 862440.
2 M. P. Cheng, J. Papenburg, M. Desjardins, S. Kanjilal, C. Quach, M. Libman, S. Dittrich and

C. P. Yansouni, *Ann. Intern. Med.*, 2020, **172**, 726–734.
3 F. Mahmoudinobar, D. Britton and J. K. Montclare, *Protein Eng., Des. Sel.*, 2021, **34**, gzab010.
4 A. Scohy, A. Anantharajah, M. Bodéus, B. Kabamba-Mukadi, A. Verroken and H. Rodriguez-Villalobos, *J. Clin. Virol.*, 2020, **129**, 104455.
5 J. K. Frediani, J. M. Levy, A. Rao, L. Bassit, J. Figueroa, M. B. Vos, A. Wood, R. Jerris, V. Leung-Pineda, M. D. Gonzalez, B. B. Rogers, M. Mavigner, R. F. Schinazi, N. Schoof, J. J. Waggoner, R. R. Kempker, P. A. Rebolledo, J. W. O'Neal, C. Stone, A. Chahroudi, C. R. Morris, A. Suessmith, J. Sullivan, S. Farmer, A. Foster, J. D. Roback, T. Ramachandra, C. Washington, K. Le, M. C. Cordero, A. Esper, E. J. Nehl, Y. F. Wang, E. A. Tyburski, G. S. Martin and W. A. Lam, *Sci. Rep.*, 2021, **11**, 14604.
6 Using antibody tests for COVID-19, **https://www.cdc.gov/coronavirus/2019-ncov/lab/resources/antibody-tests.html**, accessed: 08.28.2022.
7 H. Harpaldas, S. Arumugam, C. Campillo Rodriguez, B. A. Kumar, V. Shi and S. K. Sia, *Lab Chip*, 2021, **21**, 4517–4548.
8 J. D. Bishop, H. V. Hsieh, D. J. Gasperino and B. H. Weigl, *Lab Chip*, 2019, **19**, 2486–2499.
9 Y. Liu, L. Zhan, Z. Qin, J. Sackrison and J. C. Bischof, *ACS Nano*, 2021, **15**, 3593–3611.
10 J. Heskin, S. J. C. Pallett, A. Al-Hindawi, G. W. Davies, M. Rayment, N. Mughal, P. Randell, R. Jones and L. S. P. Moore, *Sci. Rep.*, 2022, **12**, 8811.
11 G. Koller, A. P. Morrell, R. P. Galão, S. Pickering, E. MacMahon, J. Johnson, K. Ignatyev, S. J. D. Neil, S. Elsharkawy, R. Fleck, P. M. P. Machado and O. Addison, *ACS Appl. Mater. Interfaces*, 2021, **13**, 25694–25700.
12 X. Gong, J. Cai, B. Zhang, Q. Zhao, J. Piao, W. Peng, W. Gao, D. Zhou, M. Zhao and J. Chang, *J. Mater. Chem. B*, 2017, **5**, 5079–5091.
13 R.-L. Liang, X.-P. Xu, T.-C. Liu, J.-W. Zhou, X.-G. Wang, Z.-Q. Ren, F. Hao and Y.-S. Wu, *Anal. Chim. Acta*, 2015, **891**, 277–283.
14 X.-H. Lai, R.-L. Liang, T.-C. Liu, Z.-N. Dong, Y.-S. Wu and L.-H. Li, *J. Fluoresc.*, 2016, **26**, 987–996.
15 C. Wang, X. Cheng, L. Liu, X. Zhang, X. Yang, S. Zheng, Z. Rong and S. Wang, *ACS Appl. Mater. Interfaces*, 2021, **13**, 40342–40353.
16 C. Wang, X. Yang, S. Zheng, X. Cheng, R. Xiao, Q. Li, W. Wang, X. Liu and S. Wang, *Sens. Actuators, B*, 2021, **345**, 130372.
17 R. Zou, Y. Chang, T. Zhang, F. Si, Y. Liu, Y. Zhao, Y. Liu, M. Zhang, X. Yu, X. Qiao, G. Zhu and Y. Guo, *Front. Chem.*, 2019, **7**, 18.
18 A. Nilghaz, S. M. Mousavi, J. Tian, R. Cao, R. M. Guijt and X. Wang, *ACS Appl. Nano Mater.*, 2021, **4**, 12808–12824.
19 C. N. Loynachan, M. R. Thomas, E. R. Gray, D. A. Richards, J. Kim, B. S. Miller, J. C. Brookes, S. Agarwal, V. Chudasama, R. A. McKendry and M. M. Stevens, *ACS Nano*, 2018, **12**, 279–288.
20 X. Liu, K. Wang, B. Cao, L. Shen, X. Ke, D. Cui, C. Zhong and W. Li, *Anal. Chem.*, 2021, **93**, 3626–3634.
21 A. Moyano, E. Serrano-Pertierra, M. Salvador, J. C. Martínez-García, M. Rivas and M. C. Blanco-López, *Diagnostics*, 2020, **10**, 288.
22 N. Jiang, R. Ahmed, M. Damayantharan, B. Ünal, H. Butt and A. K. Yetisen, *Adv. Healthcare Mater.*, 2019, **8**, 1900244.
23 M. Adhikari, S. Dhamane, A. E. V. Hagström, G. Garvey, W.-H. Chen, K. Kourentzi, U. Strych and R. C. Willson, *Analyst*, 2013, **138**, 5584–5587.
24 M. Adhikari, U. Strych, J. Kim, H. Goux, S. Dhamane, M.-V. Poongavanam, A. E. V. Hagström, K. Kourentzi, J. C. Conrad and R. C. Willson, *Anal. Chem.*, 2015, **87**, 11660–11665.
25 A. E. V. Hagström, G. Garvey, A. S. Paterson, S. Dhamane, M. Adhikari, M. K. Estes, U. Strych, K. Kourentzi, R. L. Atmar and R. C. Willson, *PLoS One*, 2015, **10**, e0126571.
26 J. Kim, M. Adhikari, S. Dhamane, A. E. V. Hagström, K. Kourentzi, U. Strych, R. C. Willson and J. C. Conrad, *ACS Appl. Mater. Interfaces*, 2015, **7**, 2891–2898.
27 J. Kim, R. Poling-Skutvik, J. R. C. Trabuco, K. Kourentzi, R. C. Willsona and J. C. Conrad, *Analyst*, 2017, **142**, 55–64.
28 J. Kim, B. Vu, K. Kourentzi, R. C. Willson and J. C. Conrad, *ACS Appl. Mater. Interfaces*, 2017, **9**, 6878–6884.
29 J. M. L. Bernard and M. B. Francis, *Front. Microbiol.*, 2014, **5**, 734.
30 C. M. Carmody, J. M. Goddard and S. R. Nugen, *Bioconjugate Chem.*, 2021, **32**, 466–481.
31 M. C. Smithgall, I. Scherberkova, S. Whittier and D. A. Green, *J. Clin. Virol.*, 2020, **128**, 104428.
32 B. J. Manning, W. A. Khan, J. M. Peña, E. S. Fiore, H. Boisvert, M. C. Tudino, R. E. Barney, M. K. Wilson, S. Singh, J. A. Mowatt, H. J. Thompson, G. J. Tsongalis and W. J. Blake, *Clin. Chem.*, 2022, **68**, 172–180.
33 G. T. Hermanson, *Bioconjugate Techniques*, Elsevier, 2nd edn, 2008.
34 S. Dhamane, U. Patil, M. Smith, M. Adhikari, A. Nazem, J. C. Conrad, K. Kourentzi and R. C. Willson, *Analyst*, 2021, **146**, 4835–4840.
35 N. Velappan, H. E. Fisher, E. Pesavento, L. Chasteen, S. D'Angelo, C. Kiss, M. Longmire, P. Pavlik and A. R. M. Bradbury, *Nucleic Acids Res.*, 2010, **38**, e22.
36 C. A. Schneider, W. S. Rasband and K. W. Eliceiri, *Nat. Methods*, 2012, **9**, 671–675.
37 C. B. Vogels, A. E. Watkins, C. A. Harden, D. E. Brackney, J. Shafer, J. Wang, C. Caraballo, C. C. Kalinich, I. M. Ott, J. R. Fauver, E. Kudo, P. Lu, A. Venkataraman, M. Tokuyama, A. J. Moore, M. C. Muenker, A. Casanovas-Massana, J. Fournier, S. Bermejo, M. Campbell, R. Datta, A. Nelson, Y. I. R. Team, C. S. D. Cruz, A. I. Ko, A. Iwasaki, H. M. Krumholz, J. Matheus, P. Hui, C. Liu, S. F. Farhadian and R. Sikka, *Med*, 2021, **2**, 263–280.e6.
38 B. Diao, K. Wen, J. Zhang, J. Chen, C. Han, Y. Chen, S. Wang, G. Deng, H. Zhou and Y. Wu, *Clin. Microbiol. Infect.*, 2021, **27**, 289.e1–289.e4.

39 S. Thakur, S. Sasi, S. G. Pillai, A. Nag, D. Shukla, R. Singhal, S. Phalke and G. S. K. Velu, *Front. Med.*, 2022, **9**, 815389.
40 *In vitro* diagnostics EUAs – antigen diagnostic tests for SARS-CoV-2, **https://www.fda.gov/medical-devices/coronavirus-disease-2019-covid-19-emergency-use-authorizations-medical-devices/in-vitro-diagnostics-euas-antigen-diagnostic-tests-sars-cov-2**, accessed: 12.12.2021.
41 G. L. Allen, A. K. Grahn, K. Kourentzi, R. C. Willson, S. Waldrop, J. Guo and B. K. Kay, *Front. Microbiol.*, 2022, **13**, 961093.
42 H. V. Hsieh, J. L. Dantzler and B. H. Weigl, *Diagnostics*, 2017, **7**, 29.
43 D. M. Cate, J. D. Bishop, H. V. Hsieh, V. A. Glukhova, L. F. Alonzo, H. G. Hermansky, B. Barrios-Lopez, B. D. Grant, C. E. Anderson, E. Spencer, S. Kuhn, R. Gallagher, R. Rivera, C. Bennett, S. A. Byrnes, J. T. Connelly, P. K. Dewan, D. S. Boyle, B. H. Weigl and K. P. Nichols, *ACS Omega*, 2021, **6**, 25116–25123.
44 D. A. Olsen, C. L. Brasen, S. Kahns, J. B. Madsen, H. Kierkegaard, H. Christensen, A. Jensen, T. V. Sydenham, J. K. Møller, J. S. Madsen and I. Brandslund, *Sci. Rep.*, 2021, **11**, 20323.
45 S. Pickering, R. Batra, B. Merrick, L. B. Snell, G. Nebbia, S. Douthwaite, F. Reid, A. Patel, M. T. Kia Ik, B. Patel, T. Charalampous, A. Alcolea-Medina, M. J. Lista, P. R. Cliff, E. Cunningham, J. Mullen, K. J. Doores, J. D. Edgeworth, M. H. Malim, S. J. D. Neil and R. P. Galão, *Lancet Microbe*, 2021, **2**, e461–e471.
46 G. C. K. Mak, S. S. Y. Lau, K. K. Y. Wong, N. L. S. Chow, C. S. Lau, E. T. K. Lam, R. C. W. Chan and D. N. C. Tsang, *J. Clin. Virol.*, 2020, **133**, 104684.
47 I. Petersen, A. Crozier, I. Buchan, M. J. Mina and J. W. Bartlett, *Clin. Epidemiol.*, 2021, **13**, 935–940.
48 I. Hernández-Neuta, F. Neumann, J. Brightmeyer, T. Ba Tis, N. Madaboosi, Q. Wei, A. Ozcan and M. Nilsson, *J. Intern. Med.*, 2019, **285**, 19–39.
49 I. Hussain and A. K. Bowden, *Biomed. Opt. Express*, 2021, **12**, 1974–1998.
50 O. Burggraaff, N. Schmidt, J. Zamorano, K. Pauly, S. Pascual, C. Tapia, E. Spyrakos and F. Snik, *Opt. Express*, 2019, **27**, 19075–19101.
51 P. Mertens, N. De Vos, D. Martiny, C. Jassoy, A. Mirazimi, L. Cuypers, S. Van den Wijngaert, V. Monteil, P. Melin, K. Stoffels, N. Yin, D. Mileto, S. Delaunoy, H. Magein, K. Lagrou, J. Bouzet, G. Serrano, M. Wautier, T. Leclipteux, M. Van Ranst, O. Vandenberg and L.-U. S.-C. Working Diagnostic Group, *Front. Med.*, 2020, **7**, 225.
52 D. Liu, F. Wu, Y. Cen, L. Ye, X. Shi, Y. Huang, S. Fang and L. Ma, *Mol. Immunol.*, 2021, **131**, 6–12.
53 A. N. Baker, S.-J. Richards, C. S. Guy, T. R. Congdon, M. Hasan, A. J. Zwetsloot, A. Gallo, J. R. Lewandowski, P. J. Stansfeld, A. Straube, M. Walker, S. Chessa, G. Pergolizzi, S. Dedola, R. A. Field and M. I. Gibson, *ACS Cent. Sci.*, 2020, **6**, 2046–2052.
54 B. D. Grant, C. E. Anderson, J. R. Williford, L. F. Alonzo, V. A. Glukhova, D. S. Boyle, B. H. Weigl and K. P. Nichols, *Anal. Chem.*, 2020, **92**, 11305–11309.
55 H.-Y. Kim, J.-H. Lee, M. J. Kim, S. C. Park, M. Choi, W. Lee, K. B. Ku, B. T. Kim, E. Changkyun Park, H. G. Kim and S. I. Kim, *Biosens. Bioelectron.*, 2020, **175**, 112868.
56 J.-H. Lee, M. Choi, Y. Jung, S. K. Lee, C.-S. Lee, J. Kim, J. Kim, N. H. Kim, B.-T. Kim and H. G. Kim, *Biosens. Bioelectron.*, 2021, **171**, 112715.
57 D. Liu, C. Ju, C. Han, R. Shi, X. Chen, D. Duan, J. Yan and X. Yan, *Biosens. Bioelectron.*, 2021, **173**, 112817.
58 T. Peng, X. Jiao, Z. Liang, H. Zhao, Y. Zhao, J. Xie, Y. Jiang, X. Yu, X. Fang and X. Dai, *Biosensors*, 2022, **12**, 13.
59 Y. Liu, L. Zhan, J. W. Shen, B. Baro, A. Alemany, J. Sackrison, O. Mitjá and J. C. Bischof, *ACS Appl. Nano Mater.*, 2021, **4**, 13826–13837.
60 M. Díaz-González and A. de la Escosura-Muñiz, *Anal. Bioanal. Chem.*, 2021, **413**, 4111–4117.
61 M. M. Calabretta, M. Zangheri, D. Calabria, A. Lopreside, L. Montali, E. Marchegiani, I. Trozzi, M. Guardigli, M. Mirasoli and E. Michelini, *Sensors*, 2021, **21**, 4309.